

# Triangular Lattice Model of 2D Defect Melting

Jürgen Dietel\* and Hagen Kleinert†

*Institut für Theoretische Physik, Freie Universität Berlin, Arnimallee 14, D-14195 Berlin, Germany*

(Dated: Received February 8, 2020)

We set up a harmonic lattice model for 2D defect melting which, in contrast to earlier simple-cubic models, lives on a triangular lattice. Integer-valued plastic defect gauge fields allow for the thermal generation of dislocations and disclinations. The model produces universal formulas for the melting temperature expressed in terms of the elastic constants, which are different from those derived for square lattices. They determine a Lindemann-like parameter for two-dimensional melting. In contrast to the square crystal which underwent a first-order melting transition, the triangular model melts in two steps. Our results are applied to the melting of Lennard-Jones and electron lattices.

PACS numbers: 61.72.Bb, 64.70.Dv, 64.90.+b

## I. INTRODUCTION

Melting transitions [1, 2, 3] are of both technical and theoretical interest. Under suitable experimental circumstances one can study the melting process in two dimensions (2D). If the interparticle interactions are simple, the lowest-energy crystalline order in 2D is a close-packed triangular. It is observable for electrons on a liquid-helium surface [4], for adsorbed noble-gas atoms floating on an incommensurate substrate [5], and for dense colloidal suspensions confined between parallel glass plates [6]. Simulation experiments provide us with further examples: rigid disks [7], Gaussian cores [8], and particles interacting with Lennard-Jones [9] as well as Coulomb forces (Wigner lattice) [10].

There are various theories of 2D melting [2, 3, 11, 12, 13, 14, 15, 16]. Most popular is the phenomenological theory of Halperin, Nelson and Young [12] which, inspired by the Kosterlitz and Thouless (KT) theory of vortices in superfluid films [17], explains the transition by the statistical behavior of defects. This KTHNY theory predicts melting to proceed in a sequence of two continuous KT transitions, the first caused by the unbinding of dislocations, the second by the unbinding of disclinations. Such a sequence was indeed found in some 2D crystals experimentally and by simulations.

There are also explicit models on square lattices which allow to study defect melting in detail. These models are minimal in the sense that they contain the correct harmonic elastic energy and no anharmonic terms. The defects arise from integer-valued plastic gauge fields which allow for the thermal creation and annihilation of dislocations and disclinations. The simplest such model shows only a single first-order melting transition [15]. Only after introducing an extra higher-gradient elastic term, which gives the crystal a tunable angular stiffness, the first-order transition separates into two successive KT transitions [16]. This splitting can be observed in the

laboratory, for instance in Xenon overlayer lattices on graphite [18].

Most presently investigated systems live on a triangular lattice, and these seem to melt in two steps [6, 7, 19, 20], except for the Gaussian core model. The question arises whether a minimal melting model living on a triangular lattice will undergo two successive transitions from the outset, without adding an extra higher-gradient term. It is the purpose of this paper to answer this question to the affirmative. We shall generalize the previously constructed lattice models from square lattices [2, 3, 15, 16] to triangular lattices and find, indeed, that they melt in two KT transitions.

A universal feature of all such defect models is that it is the combined separation of dislocations and disclinations which makes the melting transition first-order [15]. Dislocations alone would cause a similar phase transition as in superfluid helium, which undergoes a continuous transition.

An important virtue of the lattice defect models on square lattices was that they lead to a simple universal melting formula [2] determining the melting point in terms of the elastic constants. The result is obtained from a lowest-order approximation, which combines the high-temperature expansion of the defect contributions to the free energy density with the low-temperature expansion. The melting temperature is determined by the intersection of the two curves. This turns out to produce precisely the time-honored Lindemann criterion. In addition, however, there is a *prediction* of the universal value of the Lindemann number where melting occurs. The accuracy of the approximation was demonstrated quantitatively for square lattices in 3D and 2D [2, 21]. Recently, the results were successfully extended to face-centered and body-centered cubic lattices in 3D [22]. We shall find a similar formula for triangular lattices in 2D. The minimal lattice defect model will be constructed in Section II. From its partition function we calculate in Section III the melting temperature. In Section IV, we compare our result with the melting transition of Lennard-Jones and electron lattices. Section V discusses the melting values when taking into account nonlinear elasticity effects. In Section VI we use the model to *predict* a universal gen-

\*Electronic address: dietel@physik.fu-berlin.de

†Electronic address: kleinert@physik.fu-berlin.de

eralized Lindemann number [23] for 2D lattices.

## II. LATTICE HAMILTONIAN WITH DEFECTS

The elastic energy of a crystal in the continuum approximation is given in  $D$  dimensions by [24]

$$E_{\text{el}} = \int d^D x \left[ \frac{\mu}{4} (\partial_i u_j + \partial_j u_i)^2 + \frac{\lambda}{2} (\partial_i u_i)^2 \right], \quad (1)$$

where repeated indices are summed. The elastic constant  $\mu$  is the shear modulus, and  $\lambda$  the Lamé constant. In three dimensions, these constants are related to the elastic constants  $c_{ij}$  with lattice symmetry by  $\mu = c_{66}$  and  $\lambda = c_{11} - 2c_{66}$ . The combination  $c_{11} - c_{66}$  is the modulus of compression. In two dimensions, the fields  $u_i(x)$  ( $i = x, y$ ) are the cartesian components of the atomic displacements.

In a first step we construct a Hamiltonian on a 2D triangular lattice whose continuum elastic energy agrees with (1). Of course, this construction is not unique. We restrict the freedom by the following extension requirements:

1. The lattice derivatives  $\nabla_x$  and  $\nabla_y$  must have the continuum limits  $\partial_x$  and  $\partial_y$ , respectively.
2.  $\nabla_x, \nabla_y$  should be maximally symmetric linear combinations of the nearest neighbor lattice derivatives  $\nabla_{(l)}$ ,  $l = 1, 2, 3$  with respect to the point group of the lattice.
3.  $\nabla_x$  and  $\nabla_y$  should have the same transformation properties as  $\partial_x$  and  $\partial_y$  under the action of the point group of the lattice.

In the following we denote by  $\mathbf{e}_{(l)}$  the *oriented link vectors* of the triangular lattice which surround a triangular face of the lattice. There are three such vectors:

$$\begin{aligned} \mathbf{e}_{(1)} &= \left( \cos \frac{2\pi}{6}, \sin \frac{2\pi}{6} \right), & \mathbf{e}_{(2)} &= (-1, 0), \\ \mathbf{e}_{(3)} &= \left( \cos \frac{2\pi}{6}, -\sin \frac{2\pi}{6} \right). \end{aligned} \quad (2)$$

and three conjugate vectors  $\bar{\mathbf{e}}_{(l)} = -\mathbf{e}_{(l)}$

For each of the link vectors there exist a lattice derivative defined by

$$\begin{aligned} \nabla_{(1)} f(\mathbf{x}) &= [f(\mathbf{x} + \mathbf{e}_{(1)}) - f(\mathbf{x})] / a, \\ \nabla_{(2)} f(\mathbf{x}) &= [f(\mathbf{x}) - f(\mathbf{x} - \mathbf{e}_{(2)})] / a, \\ \nabla_{(3)} f(\mathbf{x}) &= [f(\mathbf{x} - \mathbf{e}_{(3)}) - f(\mathbf{x} + \mathbf{e}_{(1)})] / a. \end{aligned} \quad (3)$$

where  $a$  is the lattice spacing. In addition, there is a conjugate derivative  $\bar{\nabla}_{(l)} f(\mathbf{x})$  defined by  $-\nabla_{(l)} f(\mathbf{x})$  as in Eq. (3), but with the replacement  $\mathbf{e}_{(i)} \rightarrow \bar{\mathbf{e}}_{(i)}$ . From the definition follows the identity

$$(\nabla_{(1)} + \nabla_{(2)} + \nabla_{(3)}) f(\mathbf{x}) = 0 \quad (4)$$

for any function  $f(\mathbf{x})$  on the lattice sites.

The 2D point group around each lattice face is given by  $C_{3v}$  [25]. This group causes permutations of the link directions  $\mathbf{e}_{(l)}$  and the derivates  $\nabla_{(l)}$ . These can be represented by matrices which form a  $3 \times 3$ -dimensional representation of the point group  $C_{3v}$  in the space of linear combinations of the link vectors or of the lattice derivates.

We now define cartesian lattice versions  $\nabla_x$  and  $\nabla_y$  of the derivatives  $\partial_x$  and  $\partial_y$  as  $C_{3v}$ -symmetric linear combinations of the lattice derivatives  $\nabla_{(l)}$ :

$$\partial_{x,y} \rightarrow \nabla_{x,y} \equiv \frac{2}{3} e_{(l)x,y} \nabla_{(l)}. \quad (5)$$

Inserting the components from (2) these become

$$\begin{aligned} \partial_x \rightarrow \nabla_x &\equiv \frac{2}{3} \left[ \left( \frac{1}{2} \nabla_{(1)} - \nabla_{(2)} + \frac{1}{2} \nabla_{(3)} \right) \right], \\ \partial_y \rightarrow \nabla_y &\equiv \frac{2}{3} \left[ \left( \frac{\sqrt{3}}{2} \nabla_{(1)} - \frac{\sqrt{3}}{2} \nabla_{(3)} \right) \right]. \end{aligned} \quad (6)$$

It is easy to check that these fulfill the above requirements 1–3.

Without proof we mention that by using group theoretical methods (see e.g. [25]) we can show that the extension requirements 1–3 are sufficient to obtain unique lattice derivatives  $\nabla_x$  and  $\nabla_y$ . This is true for all other lattice symmetries. The only property needed for the proof is that the lattice possesses a link vector which generates all others by applying the symmetry group of the lattice.

## III. LATTICE HAMILTONIAN

It is now easy to set up the lattice version of the continuum Hamiltonian (1). We simply replace the partial derivatives by the lattice derivatives (6), and obtain

$$E_{\text{lat}} = \frac{v}{2} \sum_{\mathbf{x}} \left\{ \frac{\mu}{2} [\nabla_i u_j(\mathbf{x}) + \nabla_j u_i(\mathbf{x})]^2 + \lambda [\nabla_i u_i(\mathbf{x})]^2 \right\}. \quad (7)$$

where the sum  $\sum_{\mathbf{x}}$  runs over all lattice sites, and  $v = \sqrt{3}a^2/2$  is the area of the fundamental cell of the lattice (for the square lattice  $v = a^2$ ). As in the earlier work on square lattices [2] we shall first consider a symmetrized version of the Hamiltonian (7) which has the advantage of leading to explicit formulas for the melting transition for all  $\mu, \lambda$ . This arises by replacing  $\nabla_i$  by  $\bar{\nabla}_i$  in the  $\lambda$  term:

$$E_{\text{lat}} \approx \frac{v}{2} \sum_{\mathbf{x}} \left\{ \frac{\mu}{2} [\nabla_i u_j(\mathbf{x}) + \nabla_j u_i(\mathbf{x})]^2 + \lambda [\bar{\nabla}_i u_i(\mathbf{x})]^2 \right\}. \quad (8)$$

Without an explicit discussion in this paper we mention that one can show the difference in the results using the

symmetrized Hamiltonian (8) and the Hamiltonian (7) to be negligible for triangular as well as square lattices. The most symmetric way of writing (7) is

$$E_{\text{lat}} = \frac{\sqrt{3}a^2}{4} \sum_{\mathbf{x}} \left\{ \frac{4}{9} c_{11} \left( \sum_j \nabla_{(j)} u_{(j)} - \frac{1}{2} \sum_{i \neq j} \nabla_{(i)} u_{(j)} \right)^2 + \frac{1}{3} c_{66} \left( \sum_{kij} \epsilon_{kij} \nabla_{(i)} u_{(j)} \right)^2 + \frac{2}{3} c_{66} \left( \sum_{k \neq i \neq j} 2 \nabla_{(k)} u_{(k)} \nabla_{(i)} u_{(j)} - 2 \nabla_{(i)} u_{(k)} \nabla_{(k)} u_{(j)} - \nabla_{(k)} u_{(k)} \nabla_{(i)} u_{(i)} + \nabla_{(i)} u_{(k)} \nabla_{(k)} u_{(i)} \right) \right\}. \quad (9)$$

Here we have expanded the displacement vector in (7) in a symmetric way to  $\mathbf{u}(x) = u_{(l)}(\mathbf{x})\mathbf{e}_{(l)}$ . This representation of  $\mathbf{u}(\mathbf{x})$  is not unique due to the overcompleteness of the three link vectors (2). It becomes unique by setting  $u_{(3)} = 0$  and taking into account (4), yielding

$$E_{\text{lat}} = \frac{\sqrt{3}a^2}{4} \sum_{\mathbf{x}} \left\{ c_{11} \left( \nabla_{(1)} u_{(1)} + \nabla_{(2)} u_{(2)} \right)^2 + \frac{1}{3} c_{66} \left( \nabla_{(1)} u_{(1)} - \nabla_{(2)} u_{(2)} + 2 \nabla_{(2)} u_{(1)} - 2 \nabla_{(1)} u_{(2)} \right)^2 + 4 c_{66} \left( \nabla_{(1)} u_{(2)} \nabla_{(2)} u_{(1)} - \nabla_{(1)} u_{(1)} \nabla_{(2)} u_{(2)} \right) \right\}. \quad (10)$$

#### IV. INCLUDING DEFECT GAUGE FIELDS

With the goal of studying defect-induced melting transitions, the lattice representations (7) and (8) of linear elasticity must be extended by integer-valued defect gauge fields, the lattice version of plastic fields. From the textbook [2] we know how to do this for square lattices. The defect gauge fields reflect the fact that due to fluctuations, atoms are capable of exchanging positions with their neighbors and migrate eventually through the entire crystal. This process of self-diffusion makes it impossible to specify the displacement field uniquely. Thus, as a matter of principle, the displacement field is multi-valued. It is determined only up to an arbitrary lattice vector, since it is impossible to say whether an atom is displaced by  $\mathbf{u}(\mathbf{x})$  or by  $\mathbf{u}(\mathbf{x}) + aN_{(l)}(\mathbf{x})\mathbf{e}_{(l)}$  where  $N_{(l)}(\mathbf{x})$  is integer. The displacement vectors may have jumps across so-called *Volterra surfaces* which are described by integer-valued defect gauge fields  $n_{(lm)}(\mathbf{x})$  in the lattice model [2]. These are, in general, not symmetric.

The defect gauge fields are included into the lattice derivatives of the Hamiltonian (7) by the replacement

$$\nabla_{x,y} \mathbf{u}(\mathbf{x}) \rightarrow \frac{2}{3} e_{(l)}{}_{x,y} [\nabla_{(l)} \mathbf{u}(\mathbf{x}) - n_{(lm)}(\mathbf{x}) \mathbf{e}_{(m)}]. \quad (11)$$

The classical partition functions of the triangular crystal including dislocation and disclination degrees of freedom is then given by

$$Z = \prod_{\mathbf{x}, i} \left[ \int_{-\infty}^{\infty} \frac{du_i(\mathbf{x})}{a} \right] \sum_{\{n_{lm}(\mathbf{x})\}} \Phi[n_{lm}] \exp[-E_{\text{lat}}/k_B T]. \quad (12)$$

For simplicity, we choose periodic boundary conditions for the displacement fields  $\mathbf{u}(\mathbf{x})$ . Since defects are spanned over an integer number of fundamental cells of the lattice, the functional  $\Phi[n_{lm}]$  should restrict the range of the integer-valued gauge field  $n_{lm}$ . Furthermore, it acts also as a gauge-fixing, in such a way that only physically independent degrees of freedom are summed.

Due to the identity (4) we have the freedom to carry out the replacement  $\nabla_{x,y} \rightarrow \nabla_{x,y} + a_{x,y}(\nabla_{(1)} + \nabla_{(2)} + \nabla_{(3)})$  in (6) with some constants  $a_{x,y}$  without changing the elastic energy in (7) or (8). One can see that by considering relation (11), the resulting Hamiltonian and also the partition functions depends strongly on  $a_{x,y}$ . This is because the replacement (11) does not take into account the fact that defect lines as dislocations and disclinations are built of interstitials or vacancies, respectively, which allows only one interstitial or vacancy per fundamental cell. This restricts the *Volterra surfaces* to run through an integer number of fundamental cells. (See Fig. 1). This restriction on the defect gauge fields results in the following constraint

$$n_{(1l)}(\mathbf{x}) + n_{(2l)}(\mathbf{x}) + n_{(3l)}(\mathbf{x}) = 0, \quad (13)$$

for all  $l = 1, 2, 3$ . Here we take into account that for a dislocation the jump over the Volterra surface is constant. Disclinations are built of dislocations within our lattice model. By taking into account this constraint on the defect gauge fields the resulting partition function does not longer depend on the replacement constants  $a_{x,y}$ .

We now must identify and eliminate the gauge degrees of freedom in Eq. (12). The overcompleteness of the three basis vectors  $\mathbf{e}_{(l)}$  of the two-dimensional lattice implies that the replacement (11) leads to the same defects if the integer numbers satisfy  $n_{(li)}(\mathbf{x})\mathbf{e}_{(i)} = 0$  for  $l = 1, 2, 3$ . The rest of the gauge freedoms can be eliminated by analogy with the gauge fixing on the square lattice in the textbook [2]. Initially, the displacement fields cover only a single fundamental cell. We can extend the range to the entire crystal by fixing two of the last four components of the defect gauge field  $n_{lm}$ . One more component can be eliminated since  $E_{\text{lat}}$  depends on the derivates  $\nabla_x u_y$  and  $\nabla_y u_x$  via the sum  $\nabla_y u_x + \nabla_x u_y$ .

Finally, we must take care of the constraints due to the periodic boundary conditions. The technical aspects of the elimination of the gauge degrees of freedom are deferred to Appendix A. Eventually we arrive at the par-

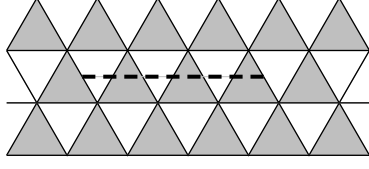


FIG. 1: Cut in a triangular lattice. For each lattice site, the shaded regions show the faces which are surrounded by the oriented link vectors (2) associated with the lattice derivates  $\nabla_{(l)}$  in Eq. (3). Dashed line indicates a *Volterra surface* crossing an integer number of fundamental cells.

tion function:

$$Z = \prod_{\mathbf{x}, i} \left[ \int_{-\infty}^{\infty} \frac{u_i(\mathbf{x})}{a} \sum_{n(\mathbf{x})=-\infty}^{\infty} \right] \times \left( (1 - \delta_{\mathbf{x}, \mathcal{B}}) + \delta_{\mathbf{x}, \mathcal{B}} \sum_{n_{(11)}(\mathbf{x}), n_{(21)}(\mathbf{x})=-\infty}^{\infty} \right) \exp[-E_{\text{lat}}/k_B T], \quad (14)$$

with the lattice energy (7) and the replacements of the lattice derivatives

$$(\nabla_x, \nabla_y) \times \mathbf{u}(\mathbf{x}) \rightarrow \frac{2}{3} (e_{(l)x}, e_{(l)y}) \times \nabla_{(l)} \mathbf{u}(\mathbf{x}) + \begin{pmatrix} 0 & \frac{1}{\sqrt{3}} n(\mathbf{x}) \\ \frac{1}{\sqrt{3}} n(\mathbf{x}) & 0 \end{pmatrix} + \delta_{\mathbf{x}, \mathcal{B}} \frac{1}{2} \begin{pmatrix} n_{(21)}(\mathbf{x}) & -\frac{1}{\sqrt{3}} n_{(21)}(\mathbf{x}) - \frac{2}{\sqrt{3}} n_{(11)}(\mathbf{x}) \\ +\sqrt{3} n_{(21)}(\mathbf{x}) & -2n_{(11)}(\mathbf{x}) - n_{(21)}(\mathbf{x}) \end{pmatrix}. \quad (15)$$

where  $\mathcal{B}$  contains the sites at the rightmost and top boundary of the sample.

The gauge degrees of freedoms are fixed by choosing  $n(\mathbf{x}) = 0$  for  $\mathbf{x} \in \mathcal{B}$ , further  $\nabla_x n(\mathbf{x}) = 0$  on the rightmost boundary  $\mathcal{B}_r$ , and  $\nabla_y n(\mathbf{x}) = 0$  on the topmost boundary  $\mathcal{B}_t$  of the model. This will be summarized by the statement

$$n(\mathbf{x}) = 0 \quad \text{for } \mathbf{x} \in \mathcal{B}'. \quad (16)$$

where  $\mathcal{B}'$  is the extended boundary consisting on the sites  $\mathcal{B}$ ,  $\mathcal{B}_t + a\mathbf{e}_{(1)}$  and  $\mathcal{B}_r + a\mathbf{e}_{(2)}$ . The boundary fields  $n_{(11)}(\mathbf{x})$  and  $n_{(21)}(\mathbf{x})$  in (15) result from the periodic boundary conditions of the displacement field  $\mathbf{u}$ , which restrict the gauge degrees of freedom.

The final partition function (14) describes a triangular crystal with harmonic elastic fluctuations and fluctuating dislocations and disclinations.

By a standard duality transformation it is possible to rewrite this partition function in a canonical form. Introducing the conjugate stress fields  $\sigma_{ij}(\mathbf{x})$  via an auxiliary

integral, we see that (17) is equal to

$$Z = \left[ \frac{\mu}{4(\lambda + \mu)} \right]^{N/2} \left( \frac{1}{2\pi\beta_{\Delta}} \right)^{3N/2} \prod_{\mathbf{x}, i \leq j} \left[ \int_{-\infty}^{\infty} d\sigma_{ij} \right] \times \prod_{\mathbf{x}} \left[ \sum_{n(\mathbf{x})=-\infty}^{\infty} \int_{-\infty}^{\infty} \frac{d\mathbf{u}(\mathbf{x})}{a} \right] \exp \left\{ -\frac{1}{2\beta} \sum_{\mathbf{x}} \left[ \sum_{i < j} \sigma_{ij}^2 + \frac{1}{2} \sum_i \sigma_{ii}^2 - \frac{\lambda}{4(\lambda + \mu)} \left( \sum_i \sigma_{ii} \right)^2 \right] \right\} \times \exp \left[ i 2\pi \sum_{\mathbf{x}} \frac{2}{3} \left[ \sum_i e_{(l)i} \nabla_{(l)} u_i \sigma_{ii} + (e_{(l)1} \nabla_{(l)} u_2 + e_{(l)2} \nabla_{(l)} u_1) \sigma_{12} \right] + H_{\sigma n} \right] \quad (17)$$

where  $\beta_{\Delta} \equiv a^2 \mu \sqrt{3} / 2k_B T (2\pi)^2$ . For details see [2].

The energy  $H_{\sigma n}$  couples the stress field  $\sigma_{ij}$  to the integer value fields  $n_{(ij)}(\mathbf{x})$ :

$$H_{\sigma n} = i 2\pi \sum_{\mathbf{x}} \frac{2}{\sqrt{3}} \sigma_{12} n(\mathbf{x}) + \ln \left[ \prod_{\mathbf{x} \in \mathcal{B}} \left[ \sum_{n_{(11)}, n_{(21)}(\mathbf{x})=-\infty}^{\infty} \right] \exp \left[ i 2\pi \left( \frac{1}{2} \sigma_{(11)}(\mathbf{x}) n_{(21)}(\mathbf{x}) - \frac{1}{2} \sigma_{(22)}(\mathbf{x}) (n_{(21)}(\mathbf{x}) + 2n_{(11)}(\mathbf{x})) + \frac{1}{\sqrt{3}} \sigma_{(12)}(\mathbf{x}) (n_{(21)}(\mathbf{x}) - n_{(11)}(\mathbf{x})) \right) \right] \right]. \quad (18)$$

This is the dual representation of (14). For very large lattices, the integer-valued fields  $n_{(11)}(\mathbf{x}), n_{(21)}(\mathbf{x})$  have, of course, no physical implications since they exists only on the boundary of the system. For the present calculations on a finite lattice they are, however, needed.

The partition function (17) corresponds to the Hamiltonian (7) including defects. The partition function for the symmetrized Hamiltonian (8) is given by the same expression with the replacement

$$\frac{\lambda}{4(\lambda + \mu)} \left( \sum_i \sigma_{ii} \right)^2 \rightarrow \frac{\lambda}{4(\lambda + \mu)} \left( \sum_i \frac{\nabla_i}{\nabla_i} \sigma_{ii} \right)^2 \quad (19)$$

in the third term of the first exponent in (17). In the following sections, we shall use the symmetrized Hamiltonian (8) corresponding to the partition function (17) with (19) as the basis for calculating physical quantities.

## V. MELTING TRANSITION

We now determine the melting temperature of the model.

### A. Lowest-Order Approximation

It has been shown in the textbook [2] that the intersection of the free energies of the two limiting curves of the high- and low- temperature expansion yields good estimates for the melting temperatures for simple cubic lattices in three dimensions and for square lattices in two dimensions (see Figs. 12.1 and 12.2 on pp. 1084–1085).

For small  $T$ , the defects are frozen out, and the partition function has the classical limit of the partition function of the Hamiltonian (8) with the derivate substitution (11) and  $n(\mathbf{x}) \equiv 0$ :

$$Z_{T \rightarrow 0} = (2\pi\beta_\Delta)^{-N} \left( \frac{\mu}{\lambda + 2\mu} \right)^{N/2} e^{-N\ell_\Delta}. \quad (20)$$

The parameter  $\ell_\Delta$  denotes the trace of the logarithm of the triangular lattice Laplacian divided by the number of sites. The Fourier transforms of the lattice derivates (3) are

$$\begin{aligned} K_{(1)} &= \frac{1}{ia} (e^{iak \cdot \mathbf{e}_{(1)}} - 1), & K_{(2)} &= \frac{1}{ia} (1 - e^{-iak \cdot \mathbf{e}_{(2)}}) \\ K_{(3)} &= \frac{1}{ia} (e^{-iak \cdot \mathbf{e}_{(2)}} - e^{iak \cdot \mathbf{e}_{(1)}}). \end{aligned} \quad (21)$$

The conjugate lattice derivatives have the complex-conjugate Fourier transforms  $\bar{K}_{(l)} = K_{(l)}^*$ . Using these, we calculate  $\ell_\Delta$  from the momentum integral

$$\begin{aligned} \ell_\Delta &= \frac{1}{2A_{BZ}} \int_{BZ} d^2k \log \left( \left[ \frac{4a^2}{9} \bar{K}_{(l)} K_{(m)} \mathbf{e}_{(l)} \cdot \mathbf{e}_{(m)} \right]^2 \right) \\ &\approx 1.22. \end{aligned} \quad (22)$$

More explicitly, the argument of the logarithm is

$$\begin{aligned} \frac{4a^2}{9} \bar{K}_{(l)} K_{(m)} \mathbf{e}_{(l)} \cdot \mathbf{e}_{(m)} \\ = \left[ 4 - \frac{4}{3} (\cos ak \cdot \mathbf{e}_{(1)} + \cos ak \cdot \mathbf{e}_{(2)} + \cos ak \cdot \mathbf{e}_{(3)}) \right]. \end{aligned} \quad (23)$$

The momentum integral in (23) runs over the 2D Brioullin zone whose area is  $A_{BZ} = (2\pi)^2 \sqrt{3}/2a^2$ . Let us compare the value (22) with the corresponding on the square lattice in Ref. [2], where the low-temperature partition function looks like (20), but with  $\ell_\Delta \approx 1.22$  replaced by  $\ell_\square \approx 1.14$ , and  $\beta_\Delta \equiv a^2 \mu \sqrt{3}/2k_B T (2\pi)^2$  by  $\beta_\square \equiv a^2 \mu / k_B T (2\pi)^2$ .

Above the melting point, the partition function is calculated from the dual representation (17). In the high-temperature limit, the defects are prolific and the sum over  $n$  can be approximated, to lowest-order, by an integral which enforces  $\sigma_{12}(\mathbf{x}) \equiv 0$ . After carrying out the integrals over the lattice displacements  $\mathbf{u}(\mathbf{x})$ , we obtain the constraint that the stress field is divergenceless. Its independent components are integrated out using the

formulas

$$\begin{aligned} \prod_{\mathbf{x}} \left[ \int_{-\infty}^{\infty} d\sigma_{11} \right] \delta \left( \frac{2a}{3} e_{(l)} \bar{\nabla}_{(l)} \sigma_{11}(\mathbf{x}) \right) \\ = \exp \left[ -\frac{N}{2A_{BZ}} \int_{BZ} d^2k \log \left( \frac{4a^2}{9} \bar{K}_{(l)} K_{(m)} e_{(l)} x e_{(m)} x \right) \right] \\ = \exp \left[ -\frac{N}{2A_{BZ}} \int_{BZ} d^2k \log (2 - 2 \cos ak \cdot \mathbf{e}_{(2)}) \right] = 1 \end{aligned} \quad (24)$$

and

$$\begin{aligned} \prod_{\mathbf{x}} \left[ \int_{-\infty}^{\infty} d\sigma_{22} \right] \delta \left( \frac{2a}{3} e_{(l)} \bar{\nabla}_{(l)} \sigma_{22}(\mathbf{x}) \right) \\ = \exp \left[ -\frac{N}{2A_{BZ}} \int_{BZ} d^2k \log \left( \frac{4a^2}{9} \bar{K}_{(l)} K_{(m)} e_{(l)} y e_{(m)} y \right) \right] \\ = \exp \left\{ -\frac{N}{2A_{BZ}} \int_{BZ} d^2k \log \left[ \frac{1}{3} (6 - 4 \cos ak \cdot \mathbf{e}_1 \right. \right. \\ \left. \left. - 4 \cos ak \cdot \mathbf{e}_3 + 2 \cos ak \cdot \mathbf{e}_2) \right] \right\} \approx \left( \frac{1}{1.15} \right)^N. \end{aligned} \quad (25)$$

The partition function  $Z$  in this limit is

$$Z_{T \rightarrow \infty} = (2\pi\beta_\Delta)^{-3N/2} \left[ \frac{\mu}{4(\lambda + \mu)} \right]^{N/2} C_\Delta^{N/2}, \quad (26)$$

where  $C_\Delta$  is the constant

$$C_\Delta \approx 0.57. \quad (27)$$

From the intersection of the high-temperature expansion (26) with the the low-temperature expansion (20) we obtain the lowest-order result for the melting transition of a triangular lattice

$$\beta_\Delta(1 + \nu) \approx \frac{1}{4\pi} e^{2\ell_\Delta} C_\Delta \approx 0.52 \quad (28)$$

where  $(1 + \nu) = 2(\lambda + \mu)/(\lambda + 2\mu)$ . This is somewhat smaller than  $\beta_\square(1 + \nu) \approx 0.81$  for the square lattice [2].

Let us now see how these results are changed by a systematic improvement of the lowest-order low- and high-temperature expansions (20) and (26).

### B. Beyond the Lowest Order

In the low-temperature regime, we include the leading contributions with nonzero defect gauge fields  $n(\mathbf{x})$  in the partition function (14). In the dual representation (17), we must take into account the integer nature of  $n(\mathbf{x})$ . This was done in Ref. [2] by reexpressing (17) in terms of the physical defect density field, which is the double-curl of the defect gauge field. Here we carry out a similar calculation for the triangular lattice. After performing, in (17), the integrals over the displacement field  $\mathbf{u}(\mathbf{x})$  and the stress fields  $\sigma_{ij}(\mathbf{x})$  we obtain the improved

low-temperature approximation  $Z = Z_{T \rightarrow 0} Z_{\Delta}^{\text{def}}$  with the defect correction factor

$$Z_{\Delta}^{\text{def}} = \prod_{\mathbf{x}} \sum_{n(\mathbf{x})=-\infty}^{\infty} \left( (1 - \delta_{\mathbf{x}, \mathcal{B}}) + \delta_{\mathbf{x}, \mathcal{B}} \sum_{n_{(12)}, n_{(11)}(\mathbf{x})=-\infty}^{\infty} \right) \times \exp \left[ -4\pi^2 \beta_{\Delta} (1 + \nu) \sum_{\mathbf{x}, \mathbf{x}'} \frac{4a^2}{9} \nabla_{(l)} e_{(l)x} \nabla_{(m)} e_{(m)y} \tilde{n}(\mathbf{x}) \times v_{\Delta}(\mathbf{x} - \mathbf{x}') \frac{4a^2}{9} \nabla_{(k)} e_{(k)x} \nabla_{(n)} e_{(n)y} \tilde{n}(\mathbf{x}') \right]. \quad (29)$$

and

$$\tilde{n}(\mathbf{x}) = \frac{2}{\sqrt{3}} n(\mathbf{x}) + \left( \frac{\nabla_{(l)} e_{(l)x}}{\nabla_{(l)} e_{(l)y}} - \frac{1}{\sqrt{3}} \right) n_{(11)}(\mathbf{x}) \delta_{\mathbf{x}, \mathcal{B}} \quad (30)$$

$$+ \left( \frac{1}{\sqrt{3}} - \frac{1}{2} \frac{\nabla_{(l)} e_{(l)y}}{\nabla_{(l)} e_{(l)x}} + \frac{1}{2} \frac{\nabla_{(l)} e_{(l)x}}{\nabla_{(l)} e_{(l)y}} \right) n_{(21)}(\mathbf{x}) \delta_{\mathbf{x}, \mathcal{B}}. \quad (31)$$

The numbers  $n(\mathbf{x})$  fulfill the boundary condition (16). In this way, we have expressed the low-temperature corrections to the harmonic partition function as a partition function of integer-valued fields  $n(\mathbf{x})$  in the bulk and two integer valued fields  $n_{(11)}(\mathbf{x})$ ,  $n_{(21)}(\mathbf{x})$  on the boundary of the sample.

The interaction potential  $v_{\Delta}$  is given by the inverse square of the triangular Laplacian

$$v_{\Delta}(\mathbf{x}) = \left[ \frac{4a^2}{9} \nabla_{(l)} \nabla_{(m)} \mathbf{e}_{(l)} \cdot \mathbf{e}_{(m)} \right]^{-2}(\mathbf{x}) \equiv \frac{1}{a^4} \square_{\Delta}^{-2}(\mathbf{x}). \quad (32)$$

It is not easy to obtain the leading-order contributions of  $Z_{\Delta}^{\text{def}}$ . This is mainly due to cancellation effects in the configuration sum coming from the interaction of the fields  $n(\mathbf{x})$  and  $n_{(11)}(\mathbf{x})$ ,  $n_{(21)}(\mathbf{x})$  on the boundary of the sample. A more efficient calculation is possible if we go over from the defect gauge fields to the *defect density field* given by

$$\eta(\mathbf{x}) = \frac{2a^2}{3} \epsilon_{kl} \epsilon_{mn} \nabla_k \nabla_m e_{(i)l} n_{(ij)}(\mathbf{x}) e_{(j)n}. \quad (33)$$

The defect field  $\eta(\mathbf{x})$  describes disclination degrees of freedoms [2]. The dislocations arise from dipoles of two nearby disclinations. The main advantage of  $\eta(\mathbf{x})$  is that it is invariant under defect gauge transformations of the integer-valued fields  $n_{(ij)}$ . Thus, we obtain for  $Z_{\Delta}^{\text{def}}$  of Eq. (29):

$$Z_{\Delta}^{\text{def}} = \prod_{\mathbf{x}} \sum_{\eta(\mathbf{x})} e^{-4\pi^2 \beta_{\Delta} (1 + \nu) \eta(\mathbf{x}) v_{\Delta}(\mathbf{x} - \mathbf{x}') \eta(\mathbf{x})}. \quad (34)$$

The sum  $\sum_{\eta(\mathbf{x})}$  runs over all different field configurations  $\eta(\mathbf{x})$  defined by (33). The values for  $v_{\Delta}(\mathbf{x})$  can be calculated via the Fourier transform

$$v_{\Delta}(\mathbf{x}) = \frac{1}{A_{\text{BZ}}} \int_{\text{BZ}} d^2 k \frac{\exp(i\mathbf{k}\mathbf{x})}{\left[ \frac{4a^2}{9} \overline{K}_{(l)} K_{(m)} \mathbf{e}_{(l)} \cdot \mathbf{e}_{(m)} \right]^2}. \quad (35)$$

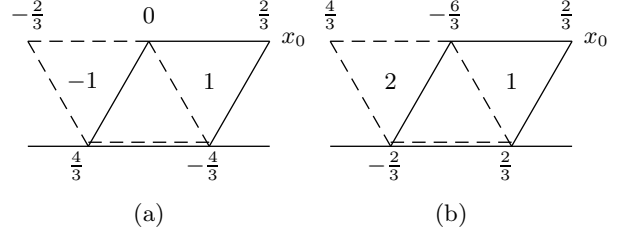


FIG. 2: Basic configurations of defect density  $\eta(\mathbf{x})$  associated with the defect gauge field  $n_{(ij)}(\mathbf{x}) = \delta_{i,1} \delta_{j,2} \delta_{\mathbf{x}, \mathbf{x}_0}$  (a), and  $n_{(ij)}(\mathbf{x}) = \delta_{i,1} \delta_{j,1} \delta_{\mathbf{x}, \mathbf{x}_0}$  (b). The numbers in the triangles denote the multiplicity of basic charges  $2/3$ .

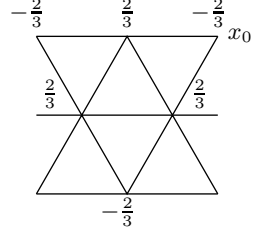


FIG. 3: Defect configuration  $\eta(\mathbf{x})$  for  $n_{(ij)}(\mathbf{x}) = (\delta_{i,2} \delta_{j,1} - \delta_{i,1} \delta_{j,2} - \delta_{i,1} \delta_{j,1}) \delta_{\mathbf{x}, \mathbf{x}_0}$ . Its contribution to the free energy is given by the first term in Eq. (36).

We fix the gauge freedom due to overcounting by setting  $n_{l3} = 0$ . Upon further using (13) we can express  $\eta(\mathbf{x})$  in terms of the fields  $n_{(ij)}$  with  $i, j = 1, 2$  only. The explicit relations are given in Eqs. (A1) and (A2). Figure 2(a) illustrates the non-zero  $\eta(\mathbf{x})$  values for  $n_{(ij)}(\mathbf{x}) = \delta_{i,1} \delta_{j,2} \delta_{\mathbf{x}, \mathbf{x}_0}$ , while 2(b) does the same thing for  $n_{(ij)}(\mathbf{x}) = \delta_{i,1} \delta_{j,1} \delta_{\mathbf{x}, \mathbf{x}_0}$ . The cases  $n_{(ij)}(\mathbf{x}) = \delta_{i,2} \delta_{j,1} \delta_{\mathbf{x}, \mathbf{x}_0}$  and  $n_{(ij)}(\mathbf{x}) = \delta_{i,2} \delta_{j,2} \delta_{\mathbf{x}, \mathbf{x}_0}$  follow from linear combinations of 2(a) and 2(b) after a clockwise rotation by an angle  $2\pi/3$ . The space of all  $\eta$ -fields are spanned by linear combinations of these four configurations modulo translations. The figure shows that the values of the  $\eta$ -field are multiples of  $2/3$  which we call *defect charges*. All  $\eta$ -configurations are composed of two neutral rhombuses which are illustrated by the dashed and straight lines in Fig 2. Besides being neutral, the rhombuses have also no dipole moments. The figure shows the multiplicity of the basic charges for both rhombuses. The fact that the  $\eta$ -fields are neutral and dipole-free agrees with the situation on the square lattice. There is one difference, however. On the triangular lattice there are neutral dipole-free charge configurations composed of multiples of basic charges  $2/3$  which cannot be obtained from an  $\eta$ -field. One simple example is a single basic rhombus shown by the dashed line in Fig. 2(a) built of defect charges  $\pm 2/3$ . The complication with respect to the square lattice where the  $\eta$ -fields are built of all neutral and dipole-free charge configurations is due to the constraint (13). Finally we mention

that the basic configuration  $\tilde{n}(\mathbf{x}) = (2/\sqrt{3}) \delta_{\mathbf{x}, \mathbf{x}_0}$  in (30) with  $\eta(\mathbf{x}) = -a^2 \nabla_x \nabla_y \tilde{n}(\mathbf{x})$  for  $\mathbf{x} \notin \mathcal{B}$  corresponds to the defect configuration 2(a).

We shall now prove that all localized  $\eta(\mathbf{x})$  fields can be built from localized  $n_{(ij)}(\mathbf{x})$ -fields if the sample is infinite. This can be seen from the fact that the line  $\mathcal{B}$  in (29) and (30) can be moved also to the middle of the system where we held fixed the boundary  $\mathcal{B}'$  in (16). This follows immediately from the considerations in Appendix A and the periodic boundary condition of the displacement fields  $u_i(\mathbf{x})$  used here. Thus, we have to take into account only a linear combination of the most localized fields  $n_{(ij)}(\mathbf{x})$  in (33) to get the leading order in the defect partition function (34).

Writing  $Z_\Delta$  as an exponential of the connected diagrams  $Z = e^{-\beta F}$ , we find the free energy of the defect fields

$$-\beta_\Delta F_\Delta^{\text{def}} \approx 2Ne^{-4\pi^2 \tilde{v}_\Delta(0)\beta_\Delta(1+\nu)} + 6Ne^{-4\pi^2 \tilde{v}_\Delta(0)\beta_\Delta \frac{4(1+\nu)}{3}} \quad (36)$$

where  $\nabla_x, \nabla_y$  are the triangular lattice derivate in (6) and

$$\tilde{v}_\Delta(\mathbf{x} - \mathbf{x}') = a^4 \nabla_x \nabla_y \nabla_{x'} \nabla_{y'} v_\Delta(\mathbf{x} - \mathbf{x}'). \quad (37)$$

By carrying out a numerical integration of the Fourier transform similar to (22) we obtain

$$\tilde{v}_\Delta(0) \approx 0.163, \quad \tilde{v}_\Delta(a\mathbf{e}_{(i)}) \approx -0.03. \quad (38)$$

These numbers are found by numerical integration of the Fourier representation similar to (35). The first term in (36) corresponds to the  $\eta(\mathbf{x})$ -configuration in Fig. 3. The second term in (36) corresponds to the  $\eta$ -configuration 2(a) in Fig. 2. The factor  $6N$  comes from the six possibilities to cover this basic  $\eta$ -configuration on the lattice, this means the configuration 2(a), the rotated configuration by angle  $2\pi/3$  and  $4\pi/3$  plus the negative of all these three configurations. The other basic diagrams are approximately a factor  $\exp[-4\pi^2 v_\Delta(0)\beta_\Delta(1+\nu)]$  smaller than the leading terms in (36). When using the mean-field value  $\beta_\Delta(1+\nu) \approx 0.6$  we obtain additive corrections which approximatively a factor 0.04 smaller than the leading terms in  $-\beta_\Delta F_\Delta^{\text{def}}$  calculated above. From this, we derive also a temperature regime for which our lowest defect configuration result can be trusted. This is given by the inequality  $4\pi^2 v_\Delta(0)\beta_\Delta(1+\nu) > 1$  resulting in  $\beta_\Delta(1+\nu) > 0.15$ .

Recall that for square lattices, the defect correction factor looks similar to (36), except that the second term is missing, and that  $\tilde{v}_\Delta$  in the first term is replaced by  $\tilde{v}^\square$ , where  $\tilde{v}^\square$  is defined by Eq. (37), with  $v^\square$  being the inverse square of the Euclidean lattice Laplacian [2]. The numerical value is  $\tilde{v}^\square(0) \approx 0.16$  [2].

Next, we consider the higher-order correction factor  $Z^{\text{stress}}$  to the high-temperature expansion of the partition function  $Z = Z_{T \rightarrow \infty} Z^{\text{stress}}$ . The correction factor is obtained by carrying out the integration over the displacement field  $\mathbf{u}(\mathbf{x})$  in Eq. (17), which makes  $\sigma_{12}(\mathbf{x})$  discrete-valued, and further summing over the defect gauge fields

$n_{(ij)}(\mathbf{x})$ . The result is

$$\begin{aligned} Z_\Delta^{\text{stress}} = & \prod_{\mathbf{x}} \left( (1 - \delta_{\mathbf{x}, \mathcal{B}'}) \left[ \sum_{\sigma_{12}(\mathbf{x}) \in \sqrt{3}\mathbb{Z}/2} \right] \right. \\ & \left. + \delta_{\mathbf{x}, \mathcal{B}'} \left[ \sum_{(\frac{1}{\sqrt{3}} - \frac{\nabla_x}{\nabla_y})\sigma_{12}(\mathbf{x}) \in \mathbb{Z}} \right] \left[ \sum_{(\frac{1}{\sqrt{3}} - \frac{1}{2}\frac{\nabla_y}{\nabla_x} + \frac{1}{2}\frac{\nabla_x}{\nabla_y})\sigma_{12}(\mathbf{x}) \in \mathbb{Z}} \right] \right. \\ & \times \exp \left[ \frac{-1}{4\beta_\Delta(1+\nu)} \sum_{\mathbf{x}, \mathbf{x}'} \sigma_{12}(\mathbf{x}) \left[ \frac{4a^2}{9} \bar{\nabla}_{(l)} \mathbf{e}_{(l)x} \bar{\nabla}_{(m)} \mathbf{e}_{(m)y} \right. \right. \\ & \left. \left. \times v_\Delta(\mathbf{x} - \mathbf{x}') \frac{4a^2}{9} \nabla_{(k)} \mathbf{e}_{(k)x'} \nabla_{(n)} \mathbf{e}_{(n)y'} \right]^{-2} \sigma_{12}(\mathbf{x}') \right]. \end{aligned} \quad (39)$$

Most of the  $\sigma_{12}$  configurations give a zero contribution to  $Z_\Delta^{\text{stress}}$  in the sum  $\sum_{\sigma_{12}(\mathbf{x}) \in \sqrt{3}\mathbb{Z}/2}$  in (39). We can extract the non-zero contributions by going to the gauge field  $\chi(\mathbf{x})$  with the definition  $\sigma_{12}(\mathbf{x}) = a^2 \nabla_x \nabla_y \chi(\mathbf{x})$ . In order to get the summation values of the fields  $\chi(\mathbf{x})$  we have to determine the lowest value  $z$  such that  $za^2 \nabla_x \nabla_y \delta_{\mathbf{x}, \mathbf{x}_0} \in \sqrt{3}\mathbb{Z}/2$  for an arbitrary lattice position  $\mathbf{x}_0$ . This value is given by  $z = 3/2$ . Neglecting boundary terms, we obtain

$$\begin{aligned} Z_\Delta^{\text{stress}} = & \prod_{\mathbf{x}} \left[ \sum_{\chi(\mathbf{x}) \in 3\mathbb{Z}/2} \right] \cdot \\ & \times \exp \left[ -\frac{1}{4\beta_\Delta(1+\nu)} \sum_{\mathbf{x}, \mathbf{x}'} \chi(\mathbf{x}) (v_\Delta)^{-2}(\mathbf{x} - \mathbf{x}') \chi(\mathbf{x}') \right] \end{aligned} \quad (40)$$

where  $v_\Delta^{-2}(\mathbf{x})$  is short for  $a^4 \square_\Delta^2(\mathbf{x})$  [recall (32)]. Numerical integration yields

$$(v_\Delta)^{-2}(0) \approx 18.5, \quad (v_\Delta)^{-2}(a\mathbf{e}_{(i)}) \approx -4.43, \quad (41)$$

so that the lowest correction to the free energy is

$$-\beta F_\Delta^{\text{stress}} \approx 2Ne^{-9(v_\Delta)^{-2}(0)/16\beta_\Delta(1+\nu)}. \quad (42)$$

The next term in the expansion of  $-\beta F_\Delta^{\text{stress}}$  is about a factor  $\exp[-9(v_\Delta)^{-2}(0)/(16\beta_\Delta(1+\nu))]$  smaller than the lowest order term in (42). By taking into account the lowest order result  $\beta_\Delta(1+\nu) \approx 0.6$  we obtain from this an extremely small factor  $e^{-20}$ . Thus, the lowest stress configuration of the high-temperature expansion in (42) can be trusted for  $\beta(1+\nu) \ll 10$ .

In the case of the square lattice [2] one gets for  $Z_\square^{\text{stress}}$  the same formula as in (42), except that the range of summation for the gauge field  $\chi(\mathbf{x})$  is  $\sum_{\chi(\mathbf{x}) \in \mathbb{Z}}$ , and that  $(v_\Delta)^{-2}$  has to be replaced by  $(v_\square)^{-2}$ . The numerical values are  $(v_\square)^{-2}(0) = 20$  and  $(v_\square)^{-2}(a\mathbf{e}_{x,y}) = -8$ .

Using the above-derived results we can now calculate the melting temperature from the intersection of the low-temperature expansion  $Z_{T \rightarrow 0} Z_\Delta^{\text{def}}$  and the high-temperature expansion  $Z_{T \rightarrow \infty} Z_\Delta^{\text{stress}}$  of the partition

function  $Z$ . Instead of (28), we find from the corrections (36) and (42) that the melting point satisfies

$$\begin{aligned} \beta(1+\nu) \approx A \exp \left[ -M_1 e^{-B_1 \beta(1+\nu)} - M_2 e^{-B_2 \beta(1+\nu)} \right] \\ \times \exp \left[ +N e^{-\frac{C}{\beta(1+\nu)}} \right] \end{aligned} \quad (43)$$

with  $\beta = \beta_{\Delta}$  in the case of the triangular lattice and  $\beta = \beta_{\square}$  for the square lattice. The parameters are

	triangular	square
$A$	0.51	0.81
$M_1$	4	4
$M_2$	12	—
$N$	4	4
$B_1$	6.45	6.31
$B_2$	8.6	—
$C$	10.4	5

(44)

Expression  $\beta F_{\Delta}/N + \ln((1-\nu)^{1/2}(1+\nu))/N$  is a function of  $\beta(1+\nu)$ . We show the corresponding curves of the low- and high-temperature expansion for the triangular lattice and the square lattice. We obtain for the square lattice that the high and low-temperature curves intersect in one point. In contrast to this, the curves of the triangular lattice do not intersect. This is caused by an enhancement of the defect contributions to the low-temperature expansions for the triangular lattice. The two curves have merely a would-be intersection near

$$\beta_{\Delta}(1+\nu) \approx 0.6, \quad (45)$$

where the distance between both curves on the  $\beta(1+\nu)$ -axis is approximatively

$$\beta_{\Delta}(1+\nu) \approx 0.05. \quad (46)$$

For a square lattice there was a definite intersection at  $\beta_{\square}(1+\nu) \approx 0.8$ . In either case, the higher-order corrections to the melting temperature are small compared to the lowest-order result (28). What is the reasons for the difference in the transition properties of the two lattices? We see from (44) that the numbers  $M_1$  and  $B_1$  are almost identical for the triangular and the square lattice. The  $\eta$ -configuration for the triangular lattice of this term is a triangle with charges  $\pm 2/3$  shown in Fig. 3. The corresponding  $\eta$ -configuration for the square lattice is given by a basic square with charges  $\pm 1$  [2]. The difference between triangular and the square lattices lies in the term proportional to  $M_2$  in (43) whose  $\eta$ -configuration is shown in Fig. 2(a). A term of this type is absent for square lattices. The defects lie on two neighboring rhombuses of charges  $\pm 2/3$ . The corresponding configuration for the square lattice would consist of two neighboring squares. The distance between the rhombuses is much smaller than that of the two nearby squares. This results in an energy reduction of the corresponding defect configuration  $\eta$  for the triangular lattice. This was the reason why this contribution was negligible for square lattices.

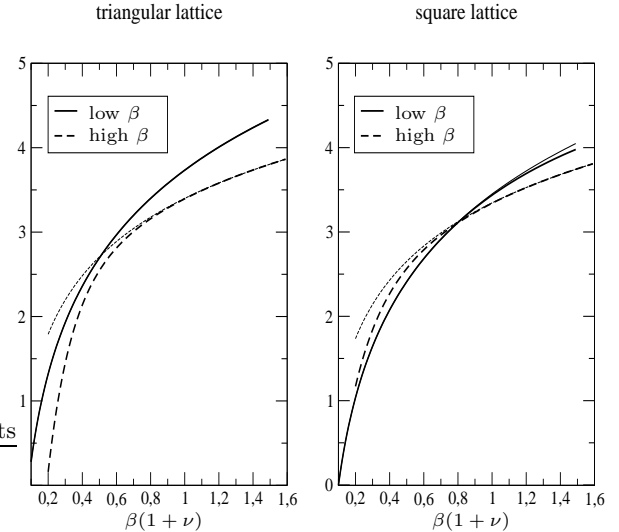


FIG. 4: Low- and high-temperature expansions of  $\beta F/N + \ln((1-\nu)^{1/2}(1+\nu))/N$  for the triangular lattice and the square lattice. The thin line curves are the lowest-order results of Section V.A, while the thick line curves take into account also the defect and stress contributions of Section V.B. Note that stress corrections are negligible.

As mentioned before, the KTHNY theory predicts a sequence of two continuous nearby melting transitions which corresponds to an unbinding of dislocations and disclinations, respectively. The behavior of the free energy shown in Fig. 4 is compatible with this prediction, considering the crudeness of the calculations. The intermediate hexatic phase between the two continuous transitions, which the model should possess, certainly unaccessible to low- and high-temperature expansions. Thus we interpret our figure to indicate two smooth phase transitions at a distance  $\Delta\beta$ , which are seen in recent computer simulations for triangular Lennard-Jones as well as electron lattices [19, 20].

The situation for the square lattice is much clearer. There is a definite intersection point in Fig. 4, indicating that the melting transition is of first order, as found by computer simulations [2, 11]. When trying to compare this result with real crystals in nature one has the difficulty that square lattices are hard to produce. They need complicated interparticle forces, and only Weber et al. [26] succeeded to do so with the help of a three-body potential. They found indeed a first-order melting transition in their simulation, in agreement with the prediction in [2, 11], and with the above conclusion.

## VI. LENNARD-JONES AND ELECTRON LATTICES IN 2D

Let us compare our results quantitatively with computer simulations of 2D Lennard-Jones as well as electron lattices. In both cases, the ground state is triangular, due to the simplicity of the interaction potential. In the Lennard-Jones lattice, the interaction potential is

$$V_{LJ}(r) = 4\epsilon \left[ \left( \frac{\sigma}{r} \right)^{12} - \left( \frac{\sigma}{r} \right)^6 \right]. \quad (47)$$

Frenkel and McTargue [27] carried out an isothermal-isochoric molecular dynamics simulation, and observed a hexatic phase in accordance with KTHNY theory. In contrast, Abraham et al. and others [28, 29] found with the help of both molecular dynamics as well as Monte-Carlo simulations that the melting transition of the Lennard-Jones lattice is of first order. The discrepancy induced simulations on larger systems, which found again KTHNY-like melting transitions [19].

To apply our model, we extract from the potential (47) the elastic moduli  $\lambda$  and  $\mu$  as follows [2]:

$$\lambda = \frac{\epsilon}{\sigma^2} \left[ 324 \left( \frac{\sigma}{a} \right)^{12} - 108 \left( \frac{\sigma}{a} \right)^6 \right], \quad (48)$$

$$\mu = \frac{\epsilon}{\sigma^2} \left[ 180 \left( \frac{\sigma}{a} \right)^{12} - 36 \left( \frac{\sigma}{a} \right)^6 \right]. \quad (49)$$

Inserting these into our result (45), we obtain for the melting temperature  $T_m$  of the triangular Lennard-Jones lattice:

$$\begin{aligned} \frac{k_B T_m}{\epsilon} &\approx 112 (\sigma^2 \rho)^2 [(\sigma^2 \rho)^3 - 0.3] \frac{1}{0.6 (2\pi)^2} \quad (50) \\ &\approx 4.725 (\sigma^2 \rho)^2 [(\sigma^2 \rho)^3 - 0.3]. \end{aligned}$$

Here  $\rho$  is the particle density  $1/v$ . Figure 5 shows  $k_B T_m/\epsilon$  as a function of  $\sigma^2 \rho$  in comparison with the two melting curves enclosing the coexisting crystal-liquid region calculated by Abraham and Barker et al. in [28]. Obviously, the value 0.6 in relation (45) is too small to agree with the simulations. This discrepancy will be removed below in Section VII.

Next, we discuss the system of a 2D electron lattice. Wigner [30] predicted in 1934 that a gas of electrons should become a triangular crystal at low temperature and density. Experimentally, this was first observed by Grimes and Adams [4] for electrons trapped on a liquid helium surface. The electrons interact via the Coulomb potential

$$V_{ee}(r) = e^2/r, \quad (51)$$

and their kinetic energy is negligible at low temperature and density. As in the case of the Lennard-Jones lattice, the ground state of the system is built of a triangular lattice [10]. Hockney and Brown [31] were the first which

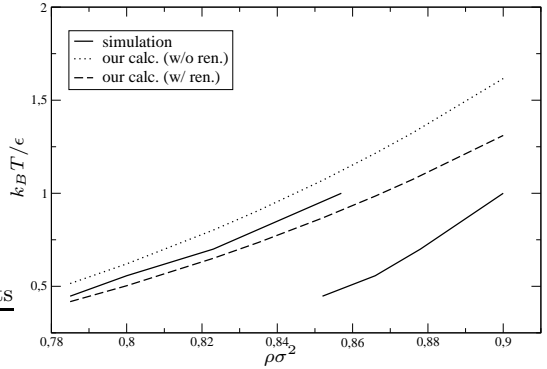


FIG. 5: Reduced melting temperature  $k_B T_m/\epsilon$  of Eq. (50) as a function of the reduced density  $\rho \sigma^2$ . The dotted line denotes the melting temperature calculated with the  $T = 0$  elastic constants. The dashed curve takes the thermal softening of the elastic constants by non-harmonic elasticity into account, calculated in Section VII. For comparison we show the melting temperature obtained by Abraham and Barker et al. [28] by simulation. The two curves of the simulation enclose the coexisting crystal-liquid region.

carry out a molecular dynamic simulation of this system. They found a  $\lambda$ -like melting transition. In contrast, Gann et al. and Kalia et al. [32] found, via Monte-Carlo and molecular dynamics studies, a first-order melting transition. Differing from both results, Morf [33] obtained a melting temperature consistent with the KTHNY theory, when he took into account the higher-order nonlinear corrections to the shear modulus. His results were reproduced by more recent simulations on larger electron lattices [20].

The elastic constants for the electron lattice are calculated in Refs. [2, 10]. The Lamé constant is infinite, so that the electron lattice has an infinite modulus of compression. The shear constant  $\mu$  is equal to

$$\mu = \eta e^2/v, \quad \eta \approx 0.245. \quad (52)$$

The simulation data yield for the melting temperature  $T_m$  the relation

$$\Gamma_m \approx 130 \pm 10, \quad (53)$$

where  $\Gamma$  is the reduced inverse temperature

$$\Gamma \equiv \sqrt{\pi} e^2 / \sqrt{v k T}. \quad (54)$$

To compare this result with our theory we insert the elastic constants into Eq. (45) and find  $\Gamma_m \approx 86.4$ , which is about 30% smaller than the simulation value. Also here, we shall remove the discrepancy in Section VII.

Concluding this section we observe that the interval  $\Delta \beta_{\Delta}(1 + \nu) \approx 0.05$  found in Fig. 4 for the triangular lattice in Eq. (46) agrees with the temperature interval of the intermediate (hexatic) phase seen in the computer simulations of both Lennard-Jones as well as electron lattices [19, 20].

## VII. ANHARMONIC CORRECTIONS TO MELTING FORMULA

The melting temperature found in the last section from formula (45) lies too high. The same problem was encountered by Thouless [34] in his calculation of the melting temperature for the electron lattice, who used the melting formula  $\beta(1 + \nu) = \sqrt{3}/\pi \approx 0.55$  where dislocations unbind in the KTHNY theory. His formula is quite close to ours in Eq. (45). It was shown by Morf in [33] that the discrepancy between the prediction with the simulated melting temperature of the electron lattice can be explained by the thermal softening of the elastic constant  $\mu$ , which he determined with the help of a computer simulation to be [recall (54)]

$$\mu(T) \approx \mu(0)(1 - 30.8/\Gamma), \quad (55)$$

where  $\mu(0)$  is the zero-temperature shear modulus (52). By using (55) one obtains from our formula (45)  $\Gamma_m \approx 117.2$ , which is now close to Morf's simulation value (53).

For 2D Lennard-Jones crystals, the thermal softening can only be estimated theoretically. We obtain a reasonable approximation of the renormalized elastic constants by observing that the thermal softening due to non linear elasticity is much stronger for the transversal than for the longitudinal sound velocity [2]. A further simplification comes from the fact [2] that the renormalization of the transversal sound is proportional to the square root of  $\mu$ , and has in first approximation a universal low-temperature law depending only on the lattice structure. This yields the approximations

$$2\mu(T) + \lambda(T) \approx 2\mu(0) + \lambda(0), \quad (56)$$

$$\mu(T) \approx \mu(0) \left[ 1 - c \frac{\mu(0)}{\beta(0)} \left( \frac{1}{\mu(0)} + \frac{1}{2\mu(0) + \lambda(0)} \right) \right]. \quad (57)$$

The constant  $c$  is the same for all lattices with the same structure. Its value can therefore be deduced from (55):

$$c_{\Delta} \approx 0.11. \quad (58)$$

Combining (56) and (57) we obtain

$$\mu(T) \approx \mu(0) \left[ 1 - \frac{c}{\beta(0)} \left( \frac{3}{2} - \frac{\nu(0)}{2} \right) \right], \quad (59)$$

$$\nu(T) \approx \nu(0) + (1 - \nu(0)) \frac{c}{\beta(0)} \left( \frac{3}{2} - \frac{\nu(0)}{2} \right). \quad (60)$$

Taking this renormalization into account, we obtain from (45) the melting formula for triangular lattices

$$\begin{aligned} \beta_{\Delta}(T)(1 + \nu(T)) &\approx \beta_{\Delta}(0)(1 + \nu(0)) - c \nu(0)(3 - \nu(0)) \\ &\approx 0.6. \end{aligned} \quad (61)$$

For the Lennard-Jones lattice where  $\nu(0) \approx 0.48$ , this leads to a melting formula

$$\beta_{\Delta}(0)(1 + \nu(0)) \approx 0.74, \quad (62)$$

rather than (45), thus lowering the melting temperature by about 20%. The dashed curve in Fig. 5 shows the resulting melting temperature for the Lennard-Jones lattice, which is compatible with the simulation data [28]. It is obtained from (50) by multiplying the right-hand side with the softening factor  $0.6/0.74 \approx 0.81$ .

## VIII. TWO-DIMENSIONAL LINDEMANN PARAMETER OF MELTING

The Lindemann parameter [23] expressed in terms of the expectation value of the lattice displacement  $\sqrt{\langle u^2(\mathbf{r}_i) \rangle}/a$  is not applicable in two dimensions, where the expectation value diverges due to excessive long-wavelength fluctuations of the displacement field. An appropriate modified Lindemann parameter in 2D is [35, 36]

$$\tilde{L} = \sqrt{\langle [u(\mathbf{x}_i) - u(\mathbf{x}_{i+1})]^2 \rangle}/a, \quad (63)$$

where  $\mathbf{x}_i$  and  $\mathbf{x}_{i+1}$  are nearest neighbors in the lattice. The correlation function of the displacement field following from the energy (8) is

$$\begin{aligned} \langle u_i(\mathbf{k}) u_j(-\mathbf{k}) \rangle &= N(k_B T) \\ &\times \frac{\overline{K}_{(l)} K_{(m)} \mathbf{e}_{(l)} \mathbf{e}_{(m)} \delta_{ij} - \frac{\lambda + \mu}{\lambda + 2\mu} \overline{K}_{(l)} K_{(m)} \mathbf{e}_{(l)} i \mathbf{e}_{(m)} j}{\mu \frac{4}{9} (\overline{K}_{(l)} K_{(m)} \mathbf{e}_{(l)} \mathbf{e}_{(m)})^2}. \end{aligned} \quad (64)$$

On square lattices, we must merely replace  $(2/3)K_{(l)}(e_{(l)})_{x,y} \rightarrow K_{x,y}$  and  $(2/3)\overline{K}_{(l)}(e_{(l)})_{x,y} \rightarrow \overline{K}_{x,y}$  [2]. From this equation we obtain for both square and triangular lattices the modified Lindemann parameter

$$\tilde{L} = \frac{1}{4\pi} \sqrt{\frac{3 - \nu(T)}{\beta(T)}}. \quad (65)$$

Let us compare our Lindemann parameter with that determined by Bedanov and Gadiyak via computer simulations for Lennard-Jones and electron lattices [35]. For the electron lattice we insert the temperature-dependent elastic constants  $\mu(T)$  of Eq. (59) and  $\nu(T) = \nu(0) = 1$  into the melting formula (61), and obtain from (65)  $\tilde{L}_{\Delta} \approx 0.20$ . The corresponding simulation value of Bedanov and Gadiyak is  $\tilde{L}_{\Delta} \approx 0.17$ , quite close to this.

Now we turn to the Lennard-Jones lattice. Using the renormalized elastic constant (60) with  $\nu(0) \approx 0.48$  and the melting formula (61) we obtain from (65) the Lindemann parameter  $\tilde{L}_{\Delta} \approx 0.20$ , again very close to the value  $\tilde{L}_{\Delta} \approx 0.18$  found in the simulations of Bedanov and Gadiyak [35].

Hence our theory yields generalized Lindemann parameters for both electron and Lennard-Jones lattices in good agreement with simulation results of Bedanov and Gadiyak [35].

### IX. SUMMARY

We have set up the simplest possible lattice model of defect melting on a two-dimensional triangular lattice. It accounts for the correct elastic fluctuations and by means of discrete-valued defect gauge fields for the fluctuations of dislocations and disclinations. The latter give rise to melting transitions, and the melting temperature follows a formula of the Lindemann type, with a modification due to the two dimensions. The value of the Lindemann parameter is predicted, and agrees with estimates obtained from computer simulations on both Lennard-Jones and electron lattices.

The melting transition is determined from the intersection of the free energies calculated once from a low-temperature expansion and once from a high-temperature expansion. While the square lattice melts in a first-order transition, the curves for the triangular lattice are compatible with two continuous transitions, as predicted by the KTHNY theory and found in computer simulations. The difference is due to the enhancement of the defect fluctuations in comparison to the square lattice caused by the smaller distance between basic nearby rhombuses on triangular lattices, in comparison to the corresponding defect configuration of two nearby squares on the square lattice. The resulting enhancement of smallest defect configurations leads to a decrease of the melting temperature.

### APPENDIX A: ELIMINATION OF THE GAUGE DEGREES OF FREEDOM

In this section we eliminate the gauge degrees of freedom in the  $n_{(lm)}$  sum of Eq. (12) enforced by the functional  $\Phi[n_{(lm)}]$ . We shall prove the following: The gauge degrees of freedom in (12) with (11) and (13) are fixed in the case that one chooses the gauge fixed integer-valued defect fields (15) with the boundary condition (16) for the bulk defect field  $n$ .

By using (4) and (13) one can transform (11) to the following expression

$$\begin{aligned} \nabla_x \mathbf{u}(\mathbf{x}) &\rightarrow -\nabla_{(2)} \mathbf{u}(\mathbf{x}) + n_{(2m)}(\mathbf{x}) \mathbf{e}_{(m)} \\ &= -\nabla_{(2)} \mathbf{u} + \begin{pmatrix} \frac{1}{2}n_{(21)} - n_{(22)} \\ \frac{\sqrt{3}}{2}n_{(21)} \end{pmatrix}, \end{aligned} \quad (\text{A1})$$

$$\begin{aligned} \nabla_y \mathbf{u}(\mathbf{x}) &\rightarrow \frac{1}{\sqrt{3}}(2\nabla_{(1)} + \nabla_{(2)})\mathbf{u}(\mathbf{x}) \\ &\quad - \frac{1}{\sqrt{3}}(2n_{(1m)}\mathbf{e}_{(m)} + n_{(2m)}\mathbf{e}_{(m)}) \\ &= \frac{1}{\sqrt{3}}(2\nabla_{(1)} + \nabla_{(2)})\mathbf{u}(\mathbf{x}) \\ &\quad + \frac{1}{\sqrt{3}} \begin{pmatrix} -n_{(11)} + 2n_{(12)} - \frac{1}{2}n_{(21)} + n_{(22)} \\ -\sqrt{3}n_{(11)} - \frac{\sqrt{3}}{2}n_{(21)} \end{pmatrix}. \end{aligned} \quad (\text{A2})$$

Here we put  $n_{(l3)} = 0$  which is possible due to the over-counting of the basis  $\mathbf{e}_{(l)}$ . Now, we can carry out the sub-

stitution of the displacement fields  $\mathbf{u}(\mathbf{x}) \rightarrow \mathbf{u}(\mathbf{x}) + a\mathbf{N}(\mathbf{x})$  in (A1) where  $a\mathbf{N}(\mathbf{x})$  is some displacement field corresponding to a jump from one lattice site to another. We determine it by the requirement that

$$a\nabla_{(2)}N_x(\mathbf{x}) = n_{(2m)}e_{(m)x} = \frac{1}{2}n_{(21)} - n_{(22)} \quad (\text{A3})$$

and

$$\begin{aligned} \frac{a}{\sqrt{3}}(2\nabla_{(1)} + \nabla_{(2)})N_y(\mathbf{x}) \\ = \frac{1}{\sqrt{3}}(2n_{(1m)}e_{(m)y} + n_{(2m)}e_{(m)y}) = n_{(11)} + \frac{1}{2}n_{(21)}. \end{aligned} \quad (\text{A4})$$

From these equations we obtain

$$a\nabla_{(l)}N_x(\mathbf{x}) \in \frac{\mathbb{Z}}{2}, \quad a\nabla_{(l)}N_y(\mathbf{x}) \in \frac{\sqrt{3}}{2}\mathbb{Z} \quad (\text{A5})$$

and

$$(2a\nabla_{(2)}N_x(\mathbf{x})) \bmod 2 = \left( \frac{2a}{\sqrt{3}}\nabla_{(2)}N_y(\mathbf{x}) \right) \bmod 2. \quad (\text{A6})$$

To derive the last equation we have used the fact that the half-integer terms on the right hand sides of (A3) and (A4) coincide. We get unique solutions of (A3) and (A4) when fixing  $N_x(\mathbf{x})$  and  $N_y(\mathbf{x})$  on one half of the boundary of the system where we now suppose that we have approximately a square sample. Thus, we can for example fix the values of  $N_x(\mathbf{x})$  and  $N_y(\mathbf{x})$  on the upper and the rightmost boundary of the sample which we denote by  $\mathcal{B}$ . Then, due to the periodic boundary conditions for the displacement field  $\mathbf{u}$  the values of  $N_x(\mathbf{x})$  and  $N_y(\mathbf{x})$  are determined on the whole boundary of the system. Because of the periodic boundary conditions for  $N_x(\mathbf{x})$  and  $N_y(\mathbf{x})$  it is not clear that the unique solution of (A3) and (A4) respects these periodic boundary conditions. That this is not generally true can be most easily seen for the square lattice [2]. Whether this is true or not depends on the values of the defect configuration on the right hand sides of (A3), (A4) and the boundary values of  $N_x(\mathbf{x})$  and  $N_y(\mathbf{x})$  on  $\mathcal{B}$ .

The values of the field  $n(\mathbf{x})$  in (15) or (17) are now given by the following expression

$$\begin{aligned} n(\mathbf{x}) &= \frac{\sqrt{3}}{2} \left[ a(\nabla_x N_y(\mathbf{x}) + \nabla_y N_x(\mathbf{x})) \right. \\ &\quad \left. + n_{(2m)}e_{(m)y} - \frac{1}{\sqrt{3}}(2n_{(1m)} + n_{(2m)})e_{(m)x} \right] \\ &= -2n_{(11)} + n_{(12)} \\ &\quad + a\nabla_{(1)}N_x(\mathbf{x}) + a\sqrt{3}\nabla_{(1)}N_y(\mathbf{x}). \end{aligned} \quad (\text{A7})$$

Here we take into account that the Hamiltonian (7) depends on the lattice derivatives of the displacement field only in the strain combination  $\nabla_x u_y + \nabla_y u_x$ . We now observe that  $\nabla_{(1)}N_{x,y}(\mathbf{x})$  can be written as a linear combination of  $\nabla_{(2)}N_{x,y}(\mathbf{x}')$  with  $y' = y$  or  $y' = y + e_{(1)}_y$  and

a lattice derivate corresponding to a rightmost boundary edge. From this, (A5), (A6), we obtain that  $n(\mathbf{x})$  on the whole lattice, given by the right-hand side of (A7), is integer valued when  $n(\mathbf{x})$  on the boundary  $\mathbf{x} \in \mathcal{B}$  have integer values.

The boundary values  $N_x(\mathbf{x})$  and  $N_y(\mathbf{x})$  on  $\mathcal{B}$  are fixed by choosing the boundary conditions (16) for  $n(\mathbf{x})$ . The

periodic boundary conditions for  $N_x(\mathbf{x})$  and  $N_y(\mathbf{x})$  on  $\mathcal{B}$  can be fixed when taking into account (A1) and (A2) only for  $\mathbf{x} \neq \mathcal{B}$ . From (A1) and (A2) we obtain further that we can fix  $n_{(22)}(\mathbf{x}) = 0$  on  $\mathcal{B}$ .

As a result we obtain the gauge-fixed path integral (14) with (15) and (16) for the triangular lattice which takes into account all defect degrees of freedom.

---

[1] W. Shockley, In *L'Etat Solide, Proceedings of Neuvième-Consil de Physique*, Brussels, 1952, Ed. R. Stoops, Solvay Institute de Physique, Brussels, Belgium

[2] H. Kleinert, *Gauge Fields in Condensed Matter, Vol. II Stresses and Defects: Differential Geometry, Crystal Melting*, World Scientific, Singapore, 1989 (readable online at [www.physik.fu-berlin.de/~kleinert/re.html#b2](http://www.physik.fu-berlin.de/~kleinert/re.html#b2)).

[3] H. Kleinert, In *Progress in Gauge Field Theory*, ed. by G. 't. Hooft et al., Plenum Press 1984, pp 373-401. ([www.physik.fu-berlin.de/~kleinert/re2.html#118](http://www.physik.fu-berlin.de/~kleinert/re2.html#118)).

[4] C. G. Grimes and G. A. Adams, Phys. Rev Lett. **42**, 795 (1979).

[5] P. A. Heiney, R. J. Birgenau, G. S. Brown, P. M. Horn, D. E. Moncton, and P. W. Stephens, Phys. Rev. Lett. **48**, 104 (1982).

[6] C. A. Murray and D. H. Van Winkle, Phys. Rev. Lett. **58**, 1200 (1987).

[7] B. J. Alder and T. E. Wainwright, Phys. Rev. **127**, 359 (1962); H. Watanabe, S. Yukawa, Y. Ozeki, and N. Ito, Phys. Rev. E **66**, 041110 (2002).

[8] F. H. Stillinger and T. A. Weber, J. Chem. Phys. **74**, 4015 (1981); T. A. Weber and F. H. Stillinger, *ibid* **74**, 4020 (1981).

[9] F. F. Abraham, Phys. Rev. **23**, 6145 (1981).

[10] L. Bonsall and A. A. Maradudin, Phys. Rev. B **15**, 1959 (1977).

[11] W. Janke and H. Kleinert, Phys. Lett. A **114**, 255 (1986) ([www.physik.fu-berlin.de/~kleinert/re2.html#135](http://www.physik.fu-berlin.de/~kleinert/re2.html#135)); W. Janke and D. Toussaint, Phys. Lett. A **116**, 387 (1986).

[12] B. I. Halperin and D. R. Nelson, Phys. Rev. Lett. **41**, 121 (1978); D. R. Nelson and B. I. Halperin, Phys. Rev. B **19**, 2457 (1979); A. P. Young, Phys. Rev. B **19**, 1855 (1979).

[13] S. T. Chui, Phys. Rev. Lett. **48**, 933 (1982).

[14] T. V. Ramakrishnan, Phys. Rev. Lett. **48**, 541 (1982).

[15] H. Kleinert, Phys. Lett. A **89**, 294 (1982). ([www.physik.fu-berlin.de/~kleinert/re1.html#89](http://www.physik.fu-berlin.de/~kleinert/re1.html#89));

[16] H. Kleinert, Phys. Lett. A **130**, 443 (1988) ([www.physik.fu-berlin.de/~kleinert/re2.html#174](http://www.physik.fu-berlin.de/~kleinert/re2.html#174)); W. Jahnke and H. Kleinert, Phys. Rev. Lett. **61**, 2344 (1988) ([www.physik.fu-berlin.de/~kleinert/re2.html#179](http://www.physik.fu-berlin.de/~kleinert/re2.html#179)); H. Kleinert, Phys. Lett. A **136**, 468 (1989) ([www.physik.fu-berlin.de/~kleinert/183](http://www.physik.fu-berlin.de/~kleinert/183)).

[17] J. M. Kosterlitz and D. J. Thouless, J. Phys. C **6**, 1181 (1973).

[18] A. Thomy and X. Duval, J. Chem. Phys. **67**, (1970) 1101.

[19] C. Urdink and J. van der Elsken, Phys. Rev. B **35**, 279 (1987); K. Chen, T. Kaplan, and M. Mostoller, Phys. Rev. Lett. **74**, 4019 (1995); F. L. Somer, Jr., G. S. Canright, T. Kaplan, K. Chen, and M. Mostoller, Phys. Rev. Lett. **79**, 3431 (1997); F. L. Somer, Jr., G. S. Canright, and T. Kaplan, Phys. Rev E **58**, 5748 (1998); A. C. Mitas, A. Z. Patashinski, A. Patrykiejew, and S. Sokolowski Phys. Rev. B **66**, 184202 (2002).

[20] S. Muto and H. Aoki, Phys. Rev. B **59**, 14911 (1999); W. J. He, T. Cui, Y. M. Ma, Z. M. Liu, and G. T. Zou, Phys. Rev. B **68**, 195104 (2003).

[21] H. Kleinert, Phys. Lett. A **95**, 381; 493 (1983) ([www.physik.fu-berlin.de/~kleinert/re2.html#101](http://www.physik.fu-berlin.de/~kleinert/re2.html#101); 104).

[22] H. Kleinert and Y. Jiang, Phys. Lett. A **313**, 152 (2003) ([www.physik.fu-berlin.de/~kleinert/re3.html#340](http://www.physik.fu-berlin.de/~kleinert/re3.html#340)).

[23] F. A. Lindemann, Phys. Z. **11**, 609 (1910).

[24] L. D. Landau and E. M. Lifshitz, *Electrodynamics of Continuous Media*, Oxford, Pergamon Press, 1960 (Course of theoretical physics 8).

[25] T. Inui, Y. Tanabe, Y. Onodera, *Group Theory and Its Applications in Physics*, Springer Verlag, Berlin Heidelberg, 1996.

[26] T. A. Weber and F. H. Stillinger, Phys. Rev. B **48**, 4351 (1993).

[27] D. Frenkel and J. P. McTague, Phys. Rev. Lett. **42**, 1632 (1979).

[28] F. F. Abraham, Phys. Rep. **80**, 339 (1981); J. A. Barker, D. Henderson, and F. F. Abraham, Physica **106A**, 226 (1981).

[29] S. W. Koch and F. F. Abraham, Phys. Rev. B **27**, 2964 (1983); J. Tobochnik and G. V. Chester, Phys. Rev. B **25**, 6778 (1982); K. J. Strandburg, J. A. Zollweg, and G. V. Chester, Phys. Rev. B **30**, 2755 (1984); S. Toxvaerd, Phys. Rev. A **24**, 2735 (1981); A. F. Bakker, C. Bruin, and H. J. Hilhorst, Phys. Rev. Lett. **52**, 449 (1984).

[30] E. Wigner, Phys. Rev. 46, 1002 (1934).

[31] R. W. Hockney and T. R. Brown, J. Phys. C **8**, 1813 (1975).

[32] R. C. Gann, S. Chakravarty, and G. V. Chester, Phys. Rev. B **20**, 326 (1979); R. K. Kalia, P. Vashista, and S. W. de Leeuw, Phys. Rev. B **23**, 4794 (1981).

[33] R. H. Morf, Phys. Rev. Lett. **43**, 931 (1979).

[34] D. J. Thouless, J. Phys. C **11**, L189 (1978).

[35] V. M. Bedanov and G. V. Gadiyak, Phys. Lett. **109A**, 289 (1985).

[36] K. Zahn, R. Lenke, and G. Maret, Phys. Rev. Lett. **82**, 2721 (1999); K. Zahn and G. Maret, Phys. Rev. Lett. **85**, 3656 (2000).